Biointerface Research in Applied Chemistry
Open-Access Journal (ISSN: 2069-5837)

Article
Volume 16, Issue 4, 2026, 113
https://doi.org/10.33263/BRIAC164.113

DFT Investigation of Nirmatrelvir Adsorption on Carbon Nanotubes for Nanodrug Delivery

Fatemeh Mollaamin [1,*], Majid Monajjemi [2]

[1] Department of Biomedical Engineering, Faculty of Engineering and Architecture, Kastamonu University, Kastamonu, Turkey; fmollaamin@kastamonu.edu.tr (F.M.);
[2] Department of Biology, Faculty of Science, Kastamonu University, Kastamonu, Turkey; m_monajjemi@yahoo.com (M.M.);
* Correspondence: fmollaamin@kastamonu.edu.tr;

Received: 5.08.2025; Accepted: 27.10.2025; Published: 15.08.2026

Abstract: Nirmatrelvir drug has been evaluated for the prevention of coronavirus. The existence of covalent features for [nirmatrelvir@(5,5) armchair SWCNT] complex has exhibited the identical energy amount and figure of the PDOS for the *p* orbitals of C, N, O and F atoms Nirmatrelvir states, onto the (5,5) armchair SWCNT have more contribution at the middle of the conduction band between –5eV to –15eV, while contribution of carbon and hydrogen sates are expanded and close together, and fluorine and nitrogen states approximately have the same contributions. ^{13}C-NMR measurements on nirmatrelvir have demonstrated the active sites of this compound by exploring the most electronegative atoms during nirmatrelvir adsorption onto the surface of (5,5) armchair SWCNT, which represent the maximal shift in TMS B3LYP/6-311+G(d,p). Electronic Circular Dichroism spectra (ECD) have been measured for the [nirmatrelvir–(5,5) armchair CNT] complex, which represents the chiroptical counterpart of the more common UV-VIS absorption spectroscopy, with a maximum adsorption band between 200 nm and 300 nm and a sharp peak at a wavelength of 248.49 nm. Data from ongoing and future trials may further advance our understanding of the effectiveness and safety of nirmatrelvir and help improve treatment guidelines for COVID-19.

Keywords: COVID–19 treatment; drug-delivery; carbon nanotube; nirmatrelvir; computational method.

1. Introduction

Nirmatrelvir ($C_{19}H_{15}F_3N_2O_3$) is an oral protease inhibitor that is active against M^{PRO}, a viral protease that plays a crucial function in viral replication by cleaving the 2 viral polyproteins [1–6]. Nanotubes with their intrinsic properties have been considered potential candidates for drug delivery carriers [7–9]. The capped ends of nanotubes may be opened by oxidation, allowing the insertion of molecules of interest into the nanotube. Carbon nanotubes (CNTs) can penetrate cells and deliver drugs directly to the cytoplasm or the nucleus. [10–12].

In this research, we have focused on nirmatrelvir adsorbed onto the surface of a (5,5) armchair SWCNT in a water medium to prevent the activity of COVID–19 (Scheme 1).

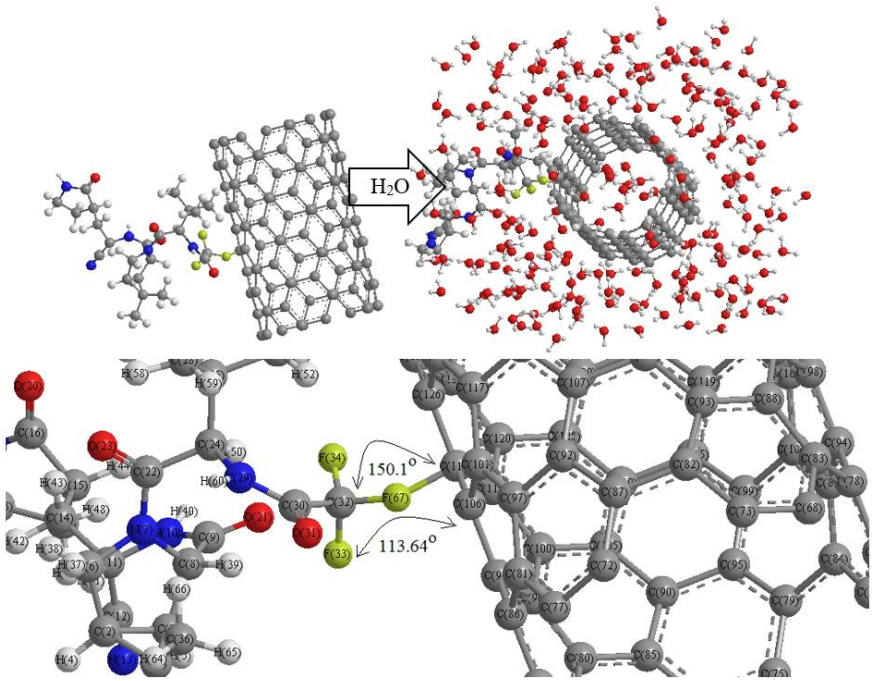

Scheme1. Adsorption of nirmatrelvir onto the surface of (5,5) armchair SWCNT in water medium.

The nirmatrelvir structure has been investigated in this study as a relatively stable drug for adsorption onto the surface of (5,5) armchair SWCNT through a drug delivery method (Scheme 1) [13,14].

Thus, a series of quantum-theoretical approaches, including DFT methods, has been used to optimize the coordination of the [nirmatrelvir@(5,5) armchair SWCNT] complex using the Gaussian 16 revision C.01 program (Scheme 1) [15].

Moreover, molnupiravir (MOL) and nirmatrelvir/ritonavir (NIR) were recently approved for the early treatment of COVID-19, but real-world data on tolerability, safety, and adverse events (AEs) remain scarce. In the real-world setting, AEs were higher than those reported in clinical trials and were particularly associated with NIR use and non-vaccination. Further analyses are needed to assess the safety of oral antivirals and to define which patient profiles may benefit most from MOL and NIR [16].

The objective of this study was to evaluate the electronic, magnetic, and spectroscopic properties of the nirmatrelvir–SWCNT complex to assess its potential as a nanocarrier.

2. Materials and Methods

The quantum method of density functional theory DFT theory proves an advantageous method for predicting chemical systems, and in order to understand its similarities and differences to other computational methods employed [17–19].

In this study, the geometry coordination has been optimized within the framework of DFT using the three-parameter Becke's exchange and Lee–Yang–Parr's correlation non-local functional [20], usually known as the B3LYP method, and a basis set of 6-311+G(d,p).

Then, the electronic structure of the adsorbed (5,5) armchair SWCNT by nirmatrelvir was measured to determine physicochemical properties (Scheme 1) [21–23].

Basically, a group of quantum theoretical methods has been run to explore some physical and chemical properties from the optimized structure of nirmatrelvir adsorbed onto the surface of (5,5) armchair SWCNT, including charge distribution, thermodynamic calculations, and nuclear magnetic resonance analysis, due to designing a drug delivery model

using the Gaussian 16 revision C.01 program [15]. Moreover, the gauge-including atomic orbitals (GIAO) have been adopted to solve the gauge problem in the calculation of nuclear magnetic shielding for the [nirmatrelvir@(5,5) armchair SWCNT] complex using density functional theory (DFT) calculations.

3. Results and Discussion

3.1. DOS and PDOS study.

The electronic structures of nirmatrelvir adsorbed on the surface of a (5,5) armchair SWCNT have been analyzed to facilitate subsequent discussion of interfacial electronic properties using the CAM-B3LYP/6-311+G (d,p) basis set.

Figure 1(a,b) shows the density of electronic states (DOS) and the projected density of states (PDOS) of [nirmatrelvir@(5,5) armchair SWCNT], respectively. The appearance of the energy states (*p*-orbitals) of fluorine (F) in nirmatrelvir increases the system's reactivity. It is clear from the figure that after adsorption on the (5,5) armchair SWCNT, there is a significant contribution of *p*-orbitals of F atoms in the unoccupied level. Based on the population analysis and DOS, it can be concluded that the F atoms of nirmatrelvir remain bonded to the (5,5) armchair SWCNT and can accept additional electrons from other atoms. Therefore, the partial DOS (PDOS) graph shows that the p states of the adsorbed F– atoms on the (5,5) armchair SWCNT dominate the conduction band (Figure 1a,b). Moreover, the presence of covalent features in the [nirmatrelvir@(5,5) armchair SWCNT] complex has yielded identical energy levels and PDOS figures for the *p* orbitals of C, N, O, and F atoms (Figure 1a,b).

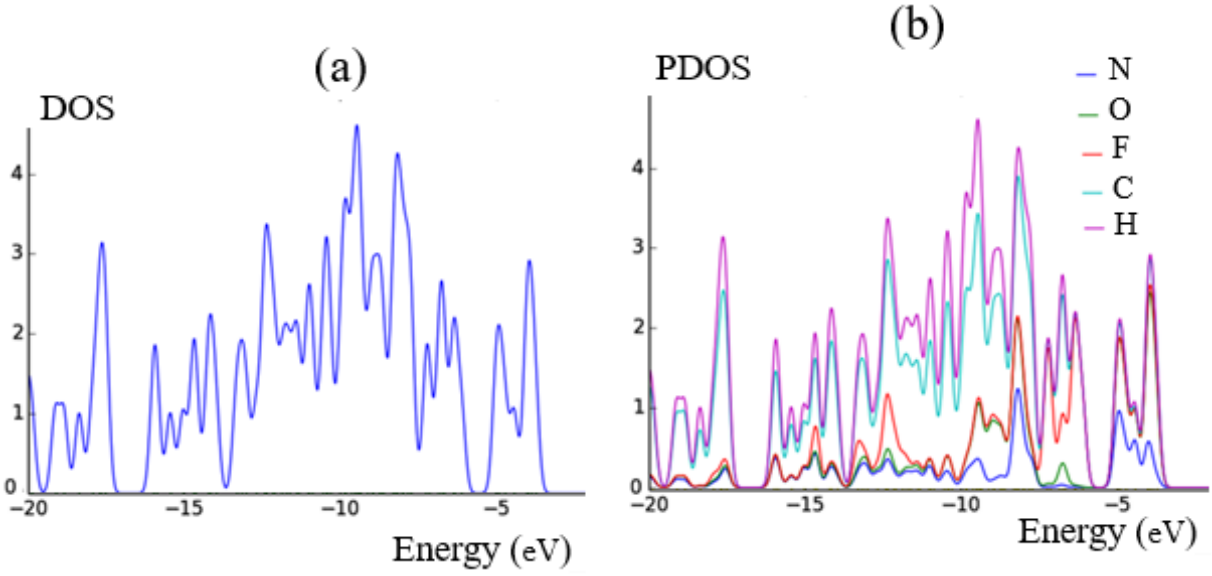

Figure 1. Electronic properties of **(a)** DOS; **(b)** PDOS for nirmatrelvir adsorbed on the (5,5) armchair SWCNT.

Figure 1a,b show that the nirmatrelvir states, respectively, adsorbed onto the (5,5) armchair SWCNT have more contribution at the middle of the conduction band between –5 eV and –15 eV, while contributions of carbon and hydrogen states are expanded and close together, and fluorine and nitrogen states approximately have the same contributions.

Therefore, the above results show that the cluster-dominant and a certain degree of covalent features can account for the increase in the semiconducting direct band gap of nirmatrelvir absorbed on the (5,5) armchair SWCNT.

3.2. NMR spectroscopy.

The NMR data of isotropic (σ_{iso}), anisotropic shielding tensor (σ_{aniso}), and eigenvalues of chemical shielding, including σ_{11}, σ_{22}, and σ_{33} (ppm) for nirmatrelvir adsorbed onto the surface of (5,5) armchair SWCNT, respectively, have been estimated (Table 1). The computed results indicate the SCF GIAO Magnetic shielding tensors in ppm for carbon, nitrogen, oxygen, and fluorine, exploring the active site of the nirmatrelvir compound as a drug for the treatment of monkeypox disease. The calculations have been performed at the B3LYP/6-311+G (d,p) level of theory using the Gaussian 16 revision C.01 program [15] and are reported in Table 1.

Table 1. SCF GIAO Magnetic shielding tensor (ppm) for nirmatrelvir adsorbed onto the surface of (5,5) armchair SWCNT in ppm using the B3LYP/6-311+G (d,p) method.

Atom	σ_{11}	σ_{22}	σ_{33}	σ_{iso}	σ_{aniso}
N11	54.5187	40.9889	303.7628	69.4184	351.5166
O18	454.9393	106.6707	446.0146	38.5318	726.8196
O19	532.1864	127.7319	412.5174	82.4670	742.4766
O29	523.3555	121.8408	428.2801	72.3054	750.8783
F31	345.7023	405.8222	422.9235	391.4827	47.1612
F32	365.8414	422.9169	428.6479	405.8021	34.2688
F33	355.3501	409.4066	415.5271	393.4279	33.1487

The [nirmatrelvir –(5,5) armchair SWCNT] complex has shown the chemical shielding, including σ_{11}, σ_{22}, σ_{33}, and σ_{iso}, σ_{aniso} (ppm) for various atoms of carbon, nitrogen, oxygen, and fluorine in the active sites of the molecule through the NMR graph (Figure 2a). The largest fluctuations have been observed in the atoms of N11, O18, O19, O29, and F31, F32, F33 (Figure 2a).

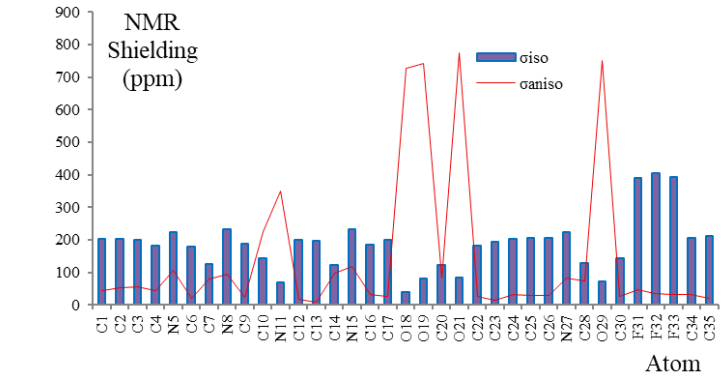

(a)

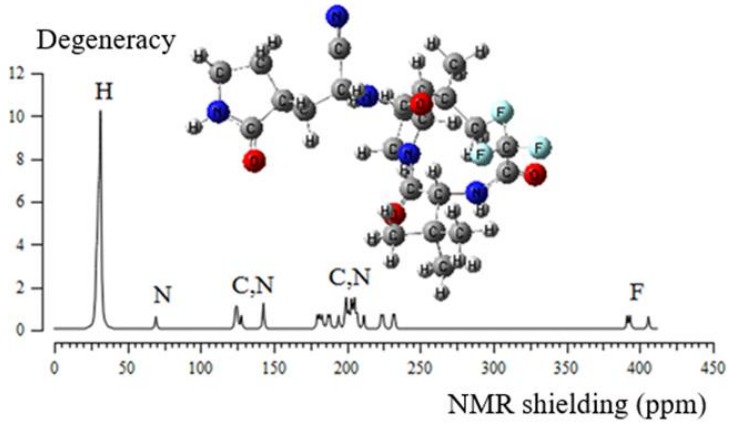

(b)

Figure 2. (a) The NMR plot of isotropic (σ_{iso}), anisotropic (σ_{aniso}) and eigenvalue shielding tensors (σ_{11}, σ_{22}, σ_{33}) calculated by level of theory B3LYP/6-311+G(d,p) for [nirmatrelvir – (5,5) armchair SWCNT] complex; **(b)** ^{13}C-NMR data on nirmatrelvir adsorbed onto the surface of (5,5) armchair SWCNT using TMS B3LYP/6-311+G(d,p) level of theory.

Moreover, the ^{13}C-NMR measurements on nirmatrelvir have demonstrated the active sites of this compound by exploring the most electronegative atoms during nirmatrelvir adsorption onto the surface of (5,5) armchair SWCNT, which represents the maximal shift in TMS B3LYP/6-311+G(d,p) (Figure 2b) [24].

Besides, the Onsager model has influenced the nuclear magnetic resonance data and chemical shielding of carbon, nitrogen, oxygen, and fluorine atoms in the [nirmatrelvir –(5,5) armchair SWCNT] complex (Figures 2a,b).

3.3. NQR analysis.

In this research, the calculated "nuclear quadrupole resonance" or "NQR" specifications extract form electrostatic properties have been calculated for nirmatrelvir towards formation of [nirmatrelvir – (5,5) armchair SWCNT] complex which is accord to the results of the "nuclear quadrupole moment", a trait of the nucleus, and the "electric field gradient" or "EFG" in the neighborhood of the nucleus [25].

As the "EFG" at the site of the nucleus in nirmatrelvir is allocated by the valence electrons twisted in the particular attachment with close nuclei of BN nanosheet, the "NQR" frequency at which transitions occur is particular for the [nirmatrelvir – (5,5) armchair SWCNT] complex (Table 2).

In this research work, the "electric potential" as the quantity of work energy through carrying over the electric charge from one position to another position in the essence of the electric field has been evaluated for the [nirmatrelvir – (5,5) armchair SWCNT] complex using "CAM-B3LYP/EPR-III,6-311+G(d,p)" level of theory (Table 2).

Table 2. The electric potential (Ep/a.u.) and Bader charge (Q/e) for elements of C, N, O, and F of the [nirmatrelvir – (5,5) armchair SWCNT] complex by CAM-B3LYP/EPR-III,6-311+G(d,p) calculation extracted from "NQR" method.

Atom	Q(e)	E_p	Electric field gradient eigenvalues		
N11	–0.19701	–18.1074	–534.665	–534.637	–534.249
O18	–0.25573	–22.0574	–812.301	–811.788	–809.209
O19	–0.23936	–22.0321	–812.351	–811.97	–809.216
O29	–0.23863	–22.0416	–812.395	–811.931	–809.259
F31	–0.11374	–26.1413	–1173.91	–1169.43	–1169.28
F32	–0.10775	–26.1299	–1173.83	–1169.37	–1169.25
F33	–0.11238	–26.1428	–1173.95	–1169.4	–1169.28

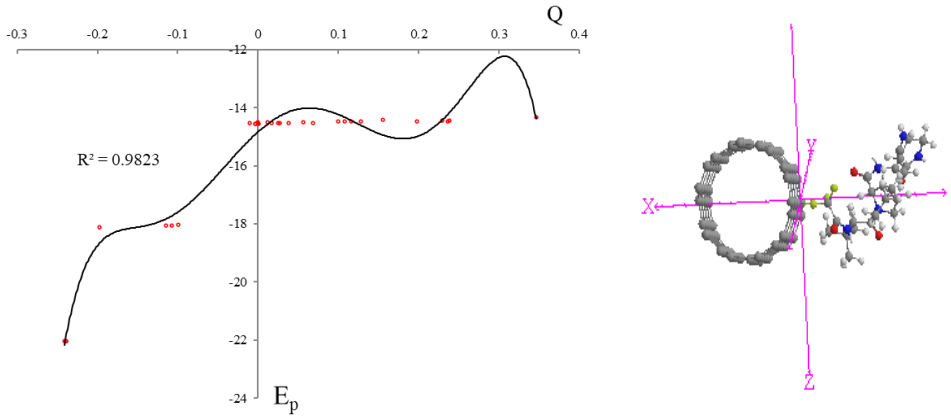

Figure 3. The electric potential versus Bader charge through NQR calculation for the adsorption of nirmatrelvir on the (5,5) armchair SWCNT using CAM–B3LYP/EPR–III, 6-311+G(d,p).

Furthermore, in Figure 3, the "electric potential" of nuclear quadrupole resonance for some atoms of carbon, nitrogen, oxygen, and fluorine in the adsorption process of nirmatrelvir

on the (5,5) armchair SWCNT is shown, which has been calculated using "CAM–B3LYP/EPR–III, 6-311+G (d,p)".

In Figure 3, the changes in electric potential for carbon, nitrogen, oxygen, and fluorine are shown in the active site of Langmuir adsorption. In fact, it has been observed that the binding of C, N, O, and F to C in the (5,5) armchair SWCNT during adsorption of nirmatrelvir resulted in an electric potential, as determined by NQR analysis, with a correlation coefficient of R2 = 0.9823 (Figure 3). It's clear that the (5,5) armchair SWCNT's capability to detect nirmatrelvir fluctuates due to its selectivity and sensitivity, indicating the efficiency of these surfaces as promising sensors.

3.4. IR method.

The calculations of the infrared (IR) spectrum have been performed for nirmatrelvir adsorbed on the surface of a (5,5) armchair SWCNT using the B3LYP method and the 6-311+G(d,p) basis set for atoms including carbon, nitrogen, oxygen, and fluorine. The IR spectrum for nirmatrelvir drug has been seen in the frequency range of about 500 cm^{-1} – 2500 cm^{-1} (Figure 4). It can be seen that the strongest allowed peaks with the highest frequency occur at about 1479.22 cm^{-1}, 1536.66 cm^{-1}, 1592.15 cm^{-1}, 1600.58 cm^{-1}, 1638.01 cm^{-1}, 1640.49 cm^{-1}, 2116.32 cm^{-1}, 2122.43 cm^{-1}, 2190.99 cm^{-1}, respectively (Figure 4).

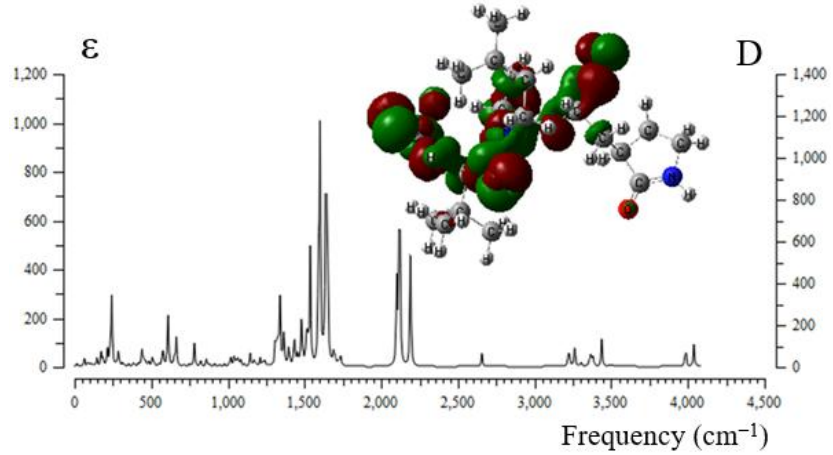

Figure 4. IR spectrum for nirmatrelvir drug adsorbed onto the surface of (5,5) armchair SWCNT using 6-311+G(d,p) calculation. Note: ε ($M^{-1}cm^{-1}$ or $Lmol^{-1}cm^{-1}$) is the absorbance unit, and D (10^{-4} esu^2 cm^2) is the dipole strength via the esu or electrostatic unit, which is a unit of charge in the cgs (centimeter-gram-second) system.

The perspective of Figure 4 suggests the reason for the observed various results frequencies of the [nirmatrelvir–(5,5) armchair CNT] complex, which presents the positions of active sites of labeled carbon, nitrogen, oxygen, and fluorine in this drug structure that transfer the charge of electrons in polar nirmatrelvir in water toward the surface of the (5,5) armchair carbon nanotube. The calculations of the relative harmonic frequencies and IR intensities in various normal modes for the [nirmatrelvir–(5,5) armchair CNT] complex using the B3LYP/6-311+G(d,p) method have been reported in Table 3 and Figure 5. Moreover, the adsorption thermodynamic properties of [nirmatrelvir–(5,5) armchair CNT] complex consist of ΔE^0_{ads}= –109.5208 × 10^{-4} (kcal mol^{-1}), ΔH^0_{ads}= –109.5207× 10^{-4} (kcal mol^{-1}), ΔG^0_{ads} = –109.5255 × 10^{-4} (kcal mol^{-1}), S^0_{ads}= 161.835 (Cal $K^{-1}mol^{-1}$), dipole moment = 4.6795 debye.

Table 3. Frequencies (cm^{-1}) and intensities (km/mol) for [nirmatrelvir–(5,5) armchair CNT] complex using B3LYP/6-311+G(d,p) method at 300K.

Normal mode	IR frequency (cm^{-1})	IR intensity (km/mol)
26	145.58	10.3659
27	173.81	16.6742
31	215.31	18.1817
32	232.86	19.2703
33	242.44	81.6183
35	284.63	16.1665
51	440.37	18.2004
56	506.82	11.0268
60	577.21	16.2637
62	610.6	59.4502
4	651.58	10.623
65	663.49	33.8809
70	781.01	27.2765
80	1019.67	10.2213
81	1040.81	12.169
92	1146.14	15.0538
100	1211.31	10.4167
105	1308.12	23.8554
106	1317.27	18.4396
108	1325.96	23.4261
109	1336.41	21.5868
110	1339.86	68.0782
113	1363.91	33.9175
115	1395.58	20.0075
118	1430.7	12.812
119	1435.35	23.5774
122	1453.95	11.4527
125	1479.22	49.9151
126	1486.6	13.0188
129	1514.2	28.2889
130	1520.1	25.3076
131	1536.66	137.3312
133	1587.36	18.105
134	1592.15	99.6933
135	1600.58	266.9787
140	1638.01	114.2942
141	1640.49	166.3732
142	1644.99	68.3656
143	1651.58	35.1909
144	1651.76	44.2988
146	1688.91	13.4197
158	1735.54	10.2007

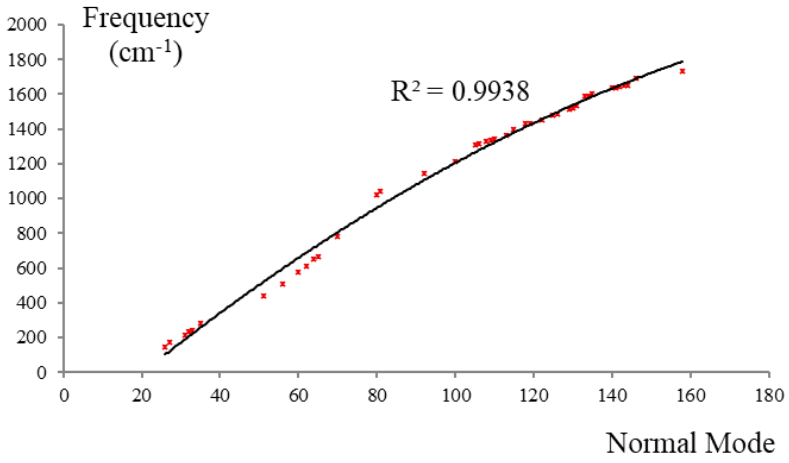

Figure 5. Harmonic frequency (cm^{-1}) versus normal mode for nirmatrelvir adsorbed onto the surface of (5,5) armchair SWCNT using B3LYP/6-311+G(d,p) quantum calculation.

Figure 5 demonstrates the linear changes of frequency versus various harmonic normal modes with a correlation coefficient R^2 = 0.9856 for nirmatrelvir drug adsorbed onto the surface of (5,5) armchair SWCNT using 6-311+G(d,p) calculation.

The results of the above observations strongly suggest that nirmatrelvir adsorbs onto the surface of a (5,5) armchair SWCNT at the B3LYP/6-311+G(d,p) level of theory in water.

3.5. HOMO and LUMO analysis and UV-VIS spectroscopy.

Ionization caused the highest occupied molecular orbital (HOMO) energy (EHOMO), and electron affinity produced the lowest unoccupied molecular orbital (LUMO) energy (E_{LUMO}). The HOMO/eV, LUMO/eV, and band energy gap (ΔE/eV) presented a pictorial explanation of the frontier molecular orbitals and their respective positive and negative zones, which were important factors for identifying the molecular characteristics of effective compounds in nirmatrelvir drug adsorbed onto the surface of (5,5) armchair SWCNT (Scheme 2).

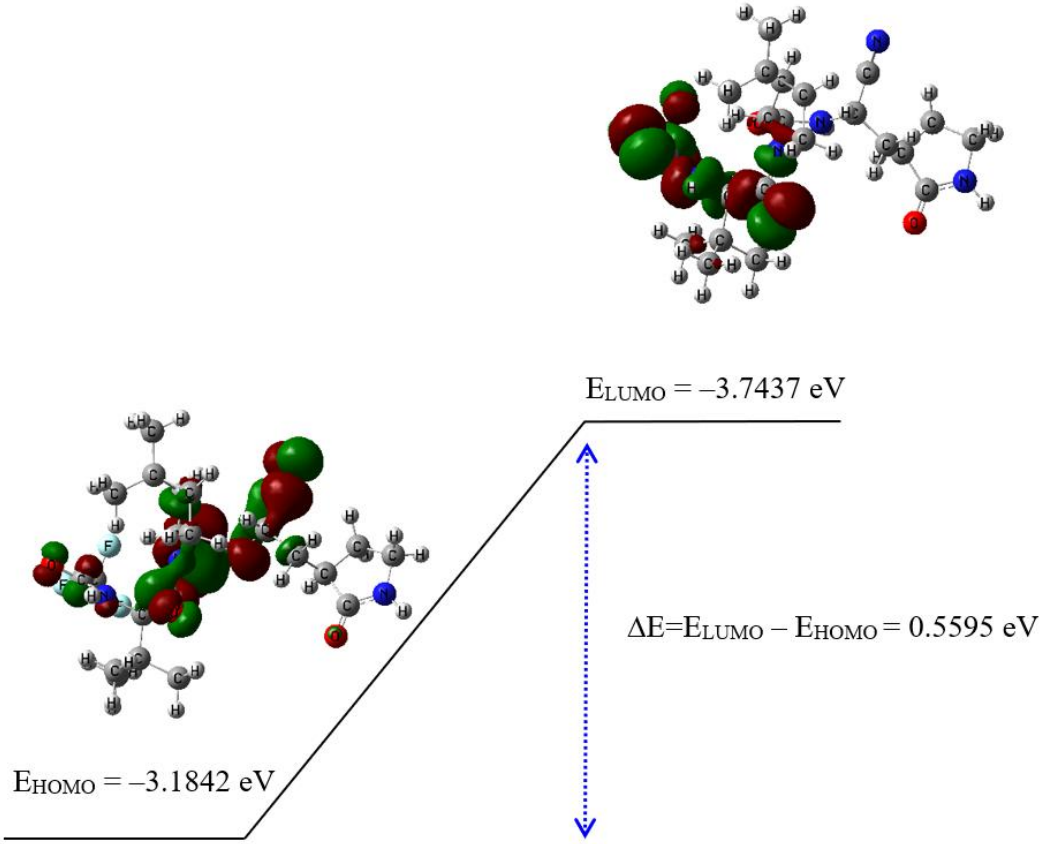

Scheme 2. The HOMO, LUMO, and band energy gap (eV) for nirmatrelvir drug adsorbed onto the surface of (5,5) armchair SWCNT.

The energy gap between HOMO and LUMO distinguishes the attributes of molecular electrical transport [26]. Through the Frank–Condon principle, the maximum absorption peak (max) depended on an ultraviolet–visible (UV-VIS) spectrum for vertical excitation. Furthermore, the vertical excitation happens from the lowest point of the PES of the ground electronic state at the minimum-energy geometry. This suggests that excitation energies by time-dependent density-functional theory (TD-DFT) should be calculated only using the method/basis set combination for which the geometry is a minimum.

In this regard, TD–DFT/6-311+G (d,p) computations were performed to identify the low-lying excited states of nirmatrelvir adsorbed onto the surface of (5,5) armchair SWCNT.

The results consist of the vertical excitation energies (E_o), oscillator strengths, and wavelengths shown in Figure 6a,b.

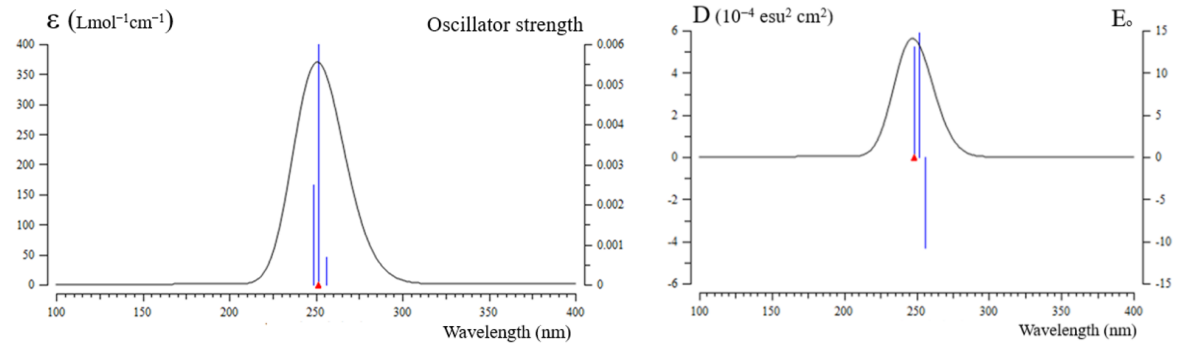

(a) **(b)**

Figure 6. (a) UV-VIS spectra; **(b)** ECD spectrum of nirmatrelvir adsorbed onto the surface of (5,5) armchair SWCNT. ε (Lmol^{-1}cm^{-1}) is the absorbance unit, and D (10^{-4} esu^2 cm^2) is the dipole strength via the esu or electrostatic unit.

In the computed ultraviolet–visible (UV-VIS) spectrum for nirmatrelvir adsorbed onto the surface of (5,5) armchair SWCNT, there was a maximum adsorption band between 200 nm and 300 nm with a sharp peak having the wavelength of 251.43 nm (Figure 6a). Moreover, Electronic Circular Dichroism spectra (ECD) have been measured for the [nirmatrelvir–(5,5) armchair CNT] complex, which represents the chiroptical counterpart of the more common UV-VIS absorption spectroscopy, with a maximum adsorption band between 200 nm and 300 nm and a sharp peak having the wavelength of 248.49 nm (Figure 6b). The results suggest that nirmatrelvir could be effective in reducing mortality and hospitalization. The results were valid in vaccinated or unvaccinated high-risk individuals with COVID-19. Data from ongoing and future trials may further advance our understanding of the effectiveness and safety of nirmatrelvir-ritonavir and help improve treatment guidelines for COVID-19.

4. Conclusions

In this work, the effect of nirmatrelvir on coronavirus disease (COVID-19) treatment has been studied by adsorption onto the surface of a (5,5) armchair SWCNT, using NMR and IR data analysis of the optimized structure. It is crucial to acknowledge that several limitations remain, and additional evidence is needed to identify the subgroups of patients who may benefit most from this treatment. It is important to highlight that observational studies are more prone to bias and confounding and therefore cannot provide conclusive evidence of causality. Data from ongoing and future randomized controlled trials may further expand our understanding of the efficacy and safety of nirmatrelvir and help improve standard treatment guidelines for COVID-19.

Author Contributions

Conceptualization, F.M.; methodology, F.M.; software, F.M.; validation, F.M. and M.M.; formal analysis, F.M. and M.M.; investigation, F.M. and M.M.; resources, F.M. and M.M.; data curation, F.M.; writing—original draft preparation, F.M.; writing—review and editing, M.M.; visualization, F.M. and M.M.; supervision, F.M.; project administration. The author has read and agreed to the published version of the manuscript.

Institutional Review Board Statement

Not applicable.

Informed Consent Statement

Not applicable.

Data Availability Statement

Not applicable.

Funding

This research received no external funding.

Acknowledgments

In successfully completing this paper and its research, the authors are grateful to Kastamonu University.

Conflict of Interest

The authors declare no conflict of interest.

References

1. Galli, M.; Migliano, F.; Fasano, V.; Silvani, A.; Passarella, D.; Citarella, A. Nirmatrelvir: From Discovery to Modern and Alternative Synthetic Approaches. *Processes* **2024**, *12*, 1242, https://doi.org/10.3390/pr12061242.
2. Mollaamin, F. Structural and Functional Characterization of Medicinal Plants as Selective Antibodies towards Therapy of COVID-19 Symptoms. *Antibodies* **2024**, *13*, 38, https://doi.org/10.3390/antib13020038
3. Trucillo, P. Advances in Drug Delivery System Designs and Therapeutics. *Processes* **2025**, *13*, 1176, https://doi.org/10.3390/pr13041176.
4. Mollaamin, F. Computational Methods in the Drug Delivery of Carbon Nanocarriers onto Several Compounds in Sarraceniaceae Medicinal Plant as Monkeypox Therapy. *Computation* **2023**, *11*, 84, https://doi.org/10.3390/computation11040084.
5. Amput, P.; Srithawong, A.; Thammachai, A.; Wongphon, S. Exploratory, Cross-Sectional Observations on Post-COVID-19 Respiratory Symptoms: A Multivariable Analysis. *COVID* **2025**, *5*, 191, https://doi.org/10.3390/covid5110191.
6. Han, Y.; Kim, D.H.; Pack, S.P. Nanomaterials in Drug Delivery: Leveraging Artificial Intelligence and Big Data for Predictive Design. *Int. J. Mol. Sci.* **2025**, *26*, 11121, https://doi.org/10.3390/ijms262211121.
7. Peleg-Evron, O.; Hen, N.; Davidovich-Pinhas, M.; Levenberg, S.; Bianco-Peled, H. Design and Characterization of Yeast Protein–Polysaccharide Bioink Blends for 3D Printing. *Polysaccharides* **2025**, *6*, 101, https://doi.org/10.3390/polysaccharides6040101.
8. Mezzano, B.A.; Bueno, M.S.; Fuertes, V.C.; Longhi, M.R.; Garnero, C. Poloxamer-Based Biomaterial as a Pharmaceutical Strategy to Improve the Ivermectin Performance. *Pharmaceutics* **2025**, *17*, 1101, https://doi.org/10.3390/pharmaceutics17091101.
9. Serrano, D.R.; Juste, F.; Anaya, B.J.; Ramirez, B.I.; Sánchez-Guirales, S.A.; Quispillo, J.M.; Hernandez, E.M.; Simon, J.A.; Trallero, J.M.; Serrano, C.; et al. Exosome-Based Drug Delivery: A Next-Generation Platform for Cancer, Infection, Neurological and Immunological Diseases, Gene Therapy and Regenerative Medicine. *Pharmaceutics* **2025**, *17*, 1336, https://doi.org/10.3390/pharmaceutics17101336.
10. Yazdani, S.; Mozaffarian, M.; Pazuki, G.; Hadidi, N.; Villate-Beitia, I.; Zárate, J.; Puras, G.; Pedraz, J.L. Carbon-Based Nanostructures as Emerging Materials for Gene Delivery Applications. *Pharmaceutics* **2024**, *16*, 288, https://doi.org/10.3390/pharmaceutics16020288.

11. Wang, Q.; Liu, Y.; Li, C.; Xu, B.; Xu, S.; Liu, B. Machine Learning-Enhanced Nanoparticle Design for Precision Cancer Drug Delivery. *Adv. Sci.* **2025**, *12*, e03138, https://doi.org/10.1002/advs.202503138.
12. Tripathy, A.; Patne, A.Y.; Mohapatra, S.; Mohapatra, S.S. Convergence of Nanotechnology and Machine Learning: The State of the Art, Challenges, and Perspectives. *Int. J. Mol. Sci.* **2024**, *25*, 12368, https://doi.org/10.3390/ijms252212368.
13. Alqarni, S.; Huwaimel, B. Predicting PLGA nanoparticle size and zeta potential in synthesis for application of drug delivery via machine learning analysis. *Sci. Rep.* **2025**, *15*, 20765, https://doi.org/10.1038/s41598-025-06872-3.
14. Kumar, P.; Agrahari, V. Emerging Trends and Translational Challenges in Drug and Vaccine Delivery. *Pharmaceutics* **2024**, *16*, 98, https://doi.org/10.3390/pharmaceutics16010098.
15. Frisch, M.J.; Trucks, G.W.; Schlegel, H.B.; Scuseria, G.E.; Robb, M.A.; Cheeseman, J.R.; Scalmani, G.; Barone, V.; Petersson, G.A.; Nakatsuji, H.; Li, X.; Caricato, M.; Marenich, A.V.; Bloino, J.; Janesko, B.G.; Gomperts, R.; Mennucci, B.; Hratchian, H.P.; Ortiz, J. V.; Izmaylov, A. F.; Sonnenberg, J.L.; Williams-Young, D.; Ding, F.; Lipparini, F.; Egidi, F.; Goings, J.; Peng, B.; Petrone, A.; Henderson, T.; Ranasinghe, D.; Zakrzewski, V.G.; Gao, J.; Rega, N.; Zheng, G.; Liang, W.; Hada, M.; Ehara, M.; Toyota, K.; Fukuda, R.; Hasegawa, J.; Ishida, M.; Nakajima, T.; Honda, Y.; Kitao, O.; Nakai, H.; Vreven, T.; Throssell, K.; Montgomery, J.A., Jr.; Peralta, J.E.; Ogliaro, F.; Bearpark, M.J.; Heyd, J.J.; Brothers, E.N.; Kudin, K.N.; Staroverov, V.N.; Keith, T.A.; Kobayashi, R.; Normand, J.; Raghavachari, K.; Rendell, A.P.; Burant, J.C.; Iyengar, S.S.; Tomasi, J.; Cossi, M.; Millam, J.M.; Klene, M.; Adamo, C.; Cammi, R.; Ochterski, J.W.; Martin, R.L.; Morokuma, K.; Farkas, O.; Foresman, J.B.; Fox, D.J. Gaussian 16, Revision C.01, Gaussian, Inc., Wallingford CT, **2016**.
16. Russo, A.; Pisaturo, M.; Cacace, C.; Troise, A.; Granata, G.; Grimaldi, P.; Allegorico, E.; Ambrisi, F.; Papillo, M.; Numis, F.G.; et al. Efficacy and Safety of Sotrovimab Versus Oral Antiviral for Early Treatment in High-Risk Patients in Omicron Era: A Multicenter Retrospective Study. *Pathogens*. **2025**, *14*, 216, https://doi.org/10.3390/pathogens14030216.
17. Elstner, M.; Cui, Q.; Gruden, M. Density Functional Theory (DFT). In Introduction to Statistical Thermodynamics: A Molecular Perspective, Elstner, M., Cui, Q., Gruden, M., Eds.; Springer International Publishing: Cham, **2024**; pp. 515-533, https://doi.org/10.1007/978-3-031-54994-6_21.
18. Mollaamin, F.; Monajjemi, M. Carbon Nanotubes as Biosensors for Releasing Conjugated Bisphosphonates–Metal Ions in Bone Tissue: Targeted Drug Delivery through the DFT Method. *C* **2023**, *9*, 61, https://doi.org/10.3390/c9020061.
19. Jin, C.; Zheng, H.; Chen, J. Advances in the Application of Graphene and Its Derivatives in Drug Delivery Systems. *Pharmaceuticals* **2025**, *18*, 1245, https://doi.org/10.3390/ph18091245.
20. Lee, C.; Yang, W.; Parr, R.G. Development of the Colle-Salvetti Correlation-Energy Formula into a Functional of the Electron Density. *Phys. Rev. B*, **1988**, *37*, 785-789, http://dx.doi.org/10.1103/PhysRevB.37.785.
21. Cho, K.S. Comparison of methodologies for the application of the Onsager variational principle. *Korea-Aust. Rheol. J.* **2025**, *37*, 43–55, https://doi.org/10.1007/s13367-024-00109-x.
22. Cho, K.S. Unified Analysis of Viscoelasticity and Viscoplasticity Using the Onsager Variational Principle. *Entropy* **2025**, *27*, 55, https://doi.org/10.3390/e27010055.
23. Wada, T.; Scarfone, A.M. Onsager's Non-Equilibrium Thermodynamics as Gradient Flow in Information Geometry. *Entropy* **2025**, *27*, 710, https://doi.org/10.3390/e27070710.
24. Hamid, S.J.; Salih, T.M.; Aziz, T.A. Rational Design, Computational Analysis and Antibacterial Activities of Synthesized Peptide-Based Molecules Targeting Quorum Sensing-Dependent Biofilm Formation in *Pseudomonas aeruginosa*. *Pharmaceuticals* **2025**, *18*, 1572, https://doi.org/10.3390/ph18101572.
25. Horace-Herron, K.L.; Raj Masna, N.V.; Swarup Bhunia; Mandal, S.; Ray, S. Nuclear Quadrupole Resonance for Substance Detection. *IEEE Access*, **2024**, *17*, 111709–111722, https://doi.org/10.1109/ACCESS.2024.3438877.
26. Abrosimov, R.; Moosmann, B. The HOMO-LUMO Gap as Discriminator of Biotic from Abiotic Chemistries. *Life* **2024**, *14*, 1330, https://doi.org/10.3390/life14101330.

Publisher's Note & Disclaimer

The statements, opinions, and data presented in this publication are solely those of the individual author(s) and contributor(s) and do not necessarily reflect the views of the publisher and/or the editor(s). The publisher and/or